Proximity Effect Correction for Fresnel Holograms on Nanophotonic Phased Arrays

Xuetong Sun* Yang Zhang† Po-Chun Huang ‡ Niloy Acharjee§ Mario Dagenais ¶
Martin Peckerar ‖ Amitabh Varshney **

University of Maryland, College Park

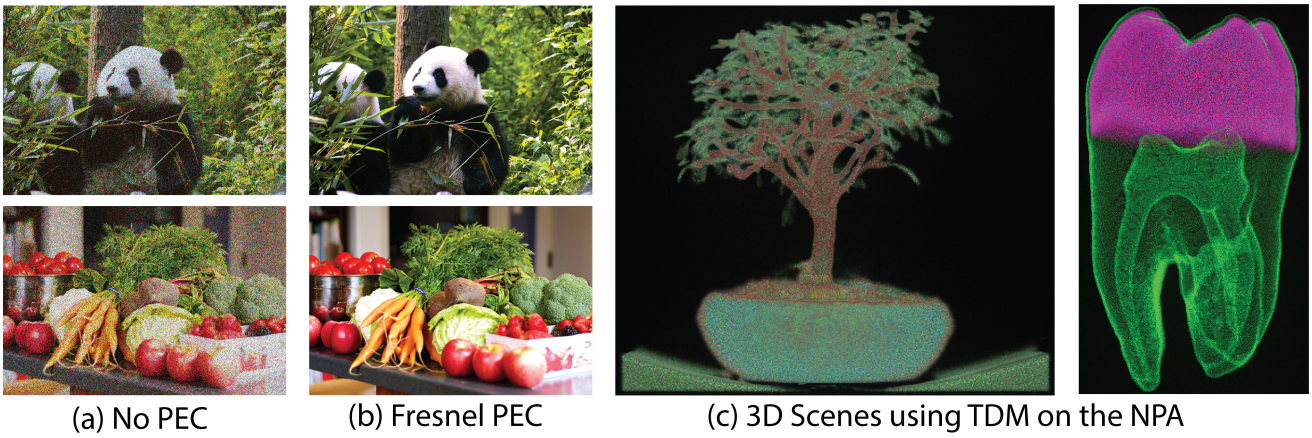

Figure 1: Thermally modulated nanophotonic phased arrays (NPAs) use temperature to modulate the phase shift of each pixel. This makes the NPAs susceptible to thermal proximity effect where heating one pixel affects the temperature of nearby pixels. This leads to reduced phase modulation accuracy and noise in the observed holograms. 2D Fresnel holograms that suffer from the proximity effect are shown in figure (a). We propose a proximity effect correction (PEC) method for 2D Fresnel holograms whose results are shown in figure (b). By leveraging the high refresh rate of the NPAs and displaying the holograms of slices of the 3D scene at their respective depths in consecutive frames with time-division multiplexing (TDM), 3D scenes can be observed, as shown in figure (c). The proximity effect level in this figure is $\sigma = 0.66$ px.

Abstract

Holographic displays and computer-generated holography offer a unique opportunity in improving optical resolutions and depth characteristics of near-eye displays. The thermally-modulated Nanophotonic Phased Array (NPA), a new type of holographic display, affords several advantages, including integrated light source and higher refresh rates, over other holographic display technologies. However, the thermal phase modulation of the NPA makes it susceptible to the thermal proximity effect where heating one pixel affects the temperature of nearby pixels. Proximity effect correction (PEC) methods have been proposed for 2D Fourier holograms in the far field but not for Fresnel holograms at user-specified depths. Here we extend an existing PEC method for the NPA to Fresnel holograms with phase-only hologram optimization and validate it through computational simulations. Our method is not only effective in correcting the proximity effect for the Fresnel holograms of 2D images at desired depths but can also leverage the fast refresh rate of the NPA to display 3D scenes with time-division multiplexing.

Keywords: Nanophotonic phased array, proximity effect correction, proximal algorithms, phase-only hologram, Fresnel hologram.

Index Terms: Computing methodologies—Image processing—; Computing methodologies—Mixed / augmented reality Computing methodologies—Virtual reality——Hardware—Displays and imagers

1 Introduction

Near-eye displays are witnessing widespread popularity with virtual and augmented reality (VR and AR) becoming mainstream. Currently, most VR and AR headsets use stereoscopic vision for depth cues and the users' eyes can only focus at one or a small number of depths. This causes the vergence-accommodation mismatch which is believed to be one of the underlying causes of visual discomfort in VR (Kramida [22]). Manual adjustments or special efforts such as in Wang *et al.* [59] are usually needed to ensure an enjoyable viewing experience in stereoscopic displays. Varifocal and light field displays have been proposed to provide a wider range of focal distances. However, varifocal displays usually involve mechanical components which makes them less durable and more difficult to manufacture. The spatial resolution and range of focal distances which a light field display can provide are limited because increasing the pixel density introduces undesirable optical diffraction artifacts.

Holographic displays rely on optical diffraction to recreate the optical waves of a scene as if they are coming from the real objects. This allows the user to naturally focus on the correct depth. Holographic displays recreate the optical waves by controlling the phase

*e-mail: xtsun@umd.edu
†yzhangdd@terpmail.umd.edu
‡hpcalex@umd.edu
§acharjee@terpmail.umd.edu
¶dage@umd.edu
‖peckerar@umd.edu
**varshney@cs.umd.edu

2642-5254/21/$31.00 ©2021 IEEE
DOI 10.1109/VR50410.2021.00058

or amplitude (or both) of the light at each pixel location. Liquid Crystal on Silicon Spatial Light Modulators (LCoS SLMs) up to millions of pixels are commercially available and are the most common holographic display. Recently, Nanophotonic Phased Array (NPA) has been demonstrated by Sun *et al.* [56] and Notaros *et al.* [41] as a new type of holographic display.

NPAs are phased arrays operating in the visible optical spectrum. The fundamental components of an NPA include an optical power distribution system, a phase modulation mechanism that is capable of controlling the phase of individual pixels, and antennas for propagating phase-modulated light into free space. One of the biggest advantages of NPAs over SLMs is the fast refresh rate. In one refresh cycle, the NPA heats each pixel to a temperature corresponding to the desired phase and lets it cool down to ambient temperature. The thermal-electric simulation on our NPA design shows that it can complete a heat-cool refresh cycle within $10\,\mu s$. This suggests that the NPAs are capable of 100kHz refresh rate and are uniquely suitable for operations such as RGB color-switching or depth scanning, as well as novel applications that make use of saccade-based perception such as in Ikeda *et al.* [16]. The NPA holographic displays also support a smaller form factor than the ones that use LCoS SLMs. The light sources can be coupled into the NPA via an optical fiber, distributed to each pixel, and emitted by the on-chip antennas making the optical operations such as beam expansion and polarization in LCoS SLMs unnecessary.

Our NPA design, as well as most other NPAs including the ones in Doylend *et al.* [7] and Sun *et al.* [56], depends on the thermo-optical effect of the materials to modulate the phase of a pixel, where the temperature adjusts the refractive index of the material. However, the use of thermal phase modulation means that heating one pixel also affects the temperature of the neighboring pixels. This phenomenon is known as the thermal proximity effect and its impact on the accuracy of phase modulation and the observed image have been shown in Sun *et al.* [57]. A simulated example of the proximity effect negatively impacting the formed images of Fresnel holograms can be seen in Fig. 1. The fact that most NPAs only have heating mechanisms but no cooling capability also makes this problem more challenging.

Sun *et al.* [57] proposed a proximity effect correction method based on the proximal algorithm. This method directly finds the phase of a phase-only hologram that minimizes the difference between the desired image and the far-field image formed under proximity effect. This method achieves good correction effectiveness but is limited to Fourier holograms. Fourier holograms are based on the Fraunhofer diffraction approximation where propagating a wavefront to a plane far away (far field) can be approximated with a Fourier transform. Fourier holograms are fast to compute and are good for reconstructing 2D images in the far field. However, the Fourier holograms calculated this way can only be observed in the far field or at two focal lengths away if placed at the focal point of a lens. Fresnel holograms, on the other hand, are based on the more accurate Fresnel diffraction approximation which is applicable closer to the source than the far field and can specify the depths of the formed imagery. An illustration of the diffraction approximations and hologram types can be seen in Fig. 2. For more detail, please refer to Goodman [14] and Voelz [58]. The closer range is more suitable for near-eye displays and the ability to specify the depth allows the users to focus on the correct focal distance. This is where holographic displays and computer-generated holography truly shine. Various methods have been proposed to calculate the 2D and 3D Fresnel holograms and display them in SLM-based holographic displays, including Maimone*et al.* [34] and Shi *et al.* [53]. No proximity effect correction method has been proposed for Fresnel holograms on the NPA.

In this paper, we present a proximity effect correction method for Fresnel holograms on nanophotonic phased arrays. This method is capable of reconstructing 2D images at user-specified depths[1]. By making use of the fast refresh rate of the NPAs, multiple 2D images at different depths can be displayed in consecutive frames, allowing users to observe a 3D scene. We show through computational simulations that our method is effective in correcting the proximity effect for Fresnel holograms and is capable of displaying 3D scenes with time-division multiplexing.

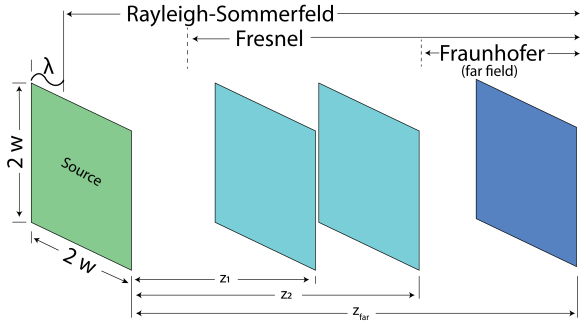

Figure 2: The Rayleigh-Sommerfeld model provides a highly accurate, but also computationally expensive, diffraction model. It is applicable within one wavelength from the source. When the propagation distance is farther, the Fresnel diffraction approximation, which is less computationally expensive than Rayleigh-Sommerfeld diffraction may be used. Holograms computed using the Fresnel diffraction are called *Fresnel holograms*. They can be reconstructed at the user-specified depths, such as z_1 and z_2. The Fresnel diffraction approximation is considered acceptable when $N_F = \frac{w^2}{\lambda z} < 30$ ([58]), where w is the radius of the source field, λ is the wavelength, and z is the propagation distance. Farther away when $N_F \ll 1$, the Fraunhofer diffraction approximation can be used where the propagation can be approximated with a Fourier transform. Holograms based on the Fraunhofer diffraction are called *Fourier holograms* and are the fastest to compute. In our NPA design, $w = 1\,\mathrm{mm}$. Given a typical green light wavelength $\lambda = 530\,\mathrm{nm}$, the Fresnel diffraction is acceptable for $z > 62.89\,\mathrm{mm}$ and Fraunhofer diffraction is suitable for $z \gg 1886.79\,\mathrm{mm}$.

2 Related Work

2.1 Nanophotonic Phased Arrays

The phased array has been an active area of research over the last century. Phased arrays operating in the microwave spectrum were first realized in the mid 1940s [11]. The invention of the lasers and the advancement in high-precision silicon photonics fabrication have laid the foundation for the nanophotonic phased arrays. Since then, the NPAs have been widely used in areas such as optical communications ([10, 18, 55]) and range finding ([38, 49]).

The use of two-dimensional NPAs as holographic displays was first demonstrated in Sun *et al.* [56]. In this NPA architecture, an optical directional coupler, a phase shifter capable of 2π phase shift, and a nanoantenna, have all been integrated into each pixel of $9\,\mu m^2$ size. An infrared image containing text was formed and observable on a 64×64 array. Zhou *et al.* [66] demonstrate the formation of 3D scenes on a 128×128 NPA operating at $1550\,\mathrm{nm}$ infrared wavelength. NPAs in the visible spectrum have also been demonstrated. A static image was shown in Raval *et al.* [50] on an NPA operating at $635\,\mathrm{nm}$ wavelength. A 3D cube was shown in Notaros *et al.* [41] which demonstrated an NPA-based near-eye holographic display.

However, dynamic phase modulation on a large scale NPA has yet to be achieved. Most of the NPAs mentioned above use static phase modulation where the phase shift of each pixel was hard-coded during fabrication. As a result, they could not display dynamic content.

[1] Example code available at https://www.cs.umd.edu/~varshney/NPA_FPEC.

Beam steering with dynamic phase modulation was demonstrated in Sun *et al.* [56] on an 8×8 array. In this paper, we address the thermal proximity effect challenge that comes with dynamic thermal modulation.

2.2 Near-Eye Displays

Head-mounted displays that rely on stereoscopic vision for depth cues such as [20, 39] can only provide one or a limited number of focal distances. This divergence from the human visual system leads to the vergence-accommodation conflict which is one of the main causes of visual discomfort according to the study by Hoffman *et al.* [15]. Varifocal and light field displays are two types of near-eye displays that are known to provide multiple or continuous focal distances. A custom varifocal display is demonstrated in Dunn *et al.* [8] with a deformable membrane controlled by airtight cavities. Commodity focus-tunable lenses have also been used in Chakravarthula *et al.* [3] and Xia *et al.* [61]. Motorized linear stages have been used to move the optical elements to adjust the focal distance in Akşit *et al.* [1] and Kim *et al.* [19]. Light field displays such as those by Lanman *et al.* [24, 60], Maimone *et al.* [33, 35], Lee *et al.* [26, 27], and Yu *et al.* [64] have also been shown to approximate the human eye accommodation. However, this approximation is limited by optical diffraction. Improving this approximation requires a larger number of pixels. Given the display's form factor, increasing the pixel density can lead to undesirable diffraction artifacts. Retinal projection displays such as those in Mi *et al.* [6,37] could circumvent the accommodation problem by directly projecting the image on the user's retina.

Holographic displays recreate the wavefront of 2D images or 3D scenes and can fully address the problem of vergence-accommodation conflict. Unlike light field displays, increasing the pixel density further improves the visual quality of holographic displays. Holographic displays based on LCoS SLMs have been demonstrated in Maimone *et al.* [34], Shi *et al.* [53], Jang *et al.* [17], and Kuo *et al.* [23]. However, the refresh rates and the form factors of the holographic displays fall short of what the NPA technology can provide.

Digital holograms must be generated to be displayed on the holographic displays. Digital holograms can be generally divided into the Fourier holograms and the Fresnel holograms based on the distance of the scene to the display and whether the distance is specified. An example of this distinction can be seen in Fig. 2. The Fourier hologram of a 2D image can be calculated efficiently with the inverse Fourier transform. Lohmann *et al.* [30] show that a binary representation of the Fourier hologram can achieve good reconstruction quality for text in a 2D image. Fresnel holograms are sometimes referred to as the physics-based holograms. They are usually calculated by summing up the interfering optical waves of the collection of spherical light sources in the scene. Directly computing the Fresnel hologram from every point is computationally intensive. Various methods have been proposed to reduce the computation such as a look-up table in Lucente [31], a distance approximation in Yoshikawa *et al.* [63], and stereograms in Lucente and Galyean [32], Xu *et al.* [62], Shi *et al.* [53] and Padmanaban *et al.* [42].

Recently, some computer-generated holography methods have been proposed that do not calculate the hologram as the wavefront from the object recorded on the hologram plane, but use optimization methods to find holograms that form the desired imagery when displayed. Chakravarthula *et al.* [4, 5] propose the Wirtinger holography that computes phase-only holograms that have better visual quality than previous methods on an SLM-based display. Peng *et al.* [47] deploy a camera in the hologram calculation process so the error of the captured image can be backpropagated to the phase-only hologram. The camera can also be used to calibrate the light transportation model of the display. To improve the long hologram calculation time, Eybposh *et al.* [9] and Peng *et al.* [47] use deep neural networks to deliver high-quality holograms in real-time.

We refer interested readers to surveys by Koulieris *et al.* [21] and Kramida [22] for more details on near-eye displays and vergence-accommodation conflict.

2.3 Proximity Effect Correction

The proximity effect is present in several processes in addition to thermal phase modulation and various proximity effect correction methods have been proposed.

In E-beam lithography, the energy deposited at one location may spill into the surroundings. Parikh [43] and Peckerar *et al.* [46] propose a proximity effect correction method based on solving a set of linear equations defined by proximity effect. To address negative values that arise from solution of linear equations, which are physically implausible, Peckerar *et al.* [36, 46] propose to add a regularizer term to the cost functions in the deconvolution problem to penalize negative entries. Non-negative matrix factorization in Lee and Seung [25] may also be used to address the non-negative constraint on the solution. We refer interested readers to the survey by Li [28] for more PEC methods in E-beam lithography.

In voltage cross-talk in LCoS SLMs, the voltage applied to one pixel may affect nearby pixels. Persson *et al.* [48] and Gemayel *et al.* [12] mitigate voltage cross-talk by taking it into consideration at each iteration of the Gerchberg-Saxton phase retrieval algorithm [13].

In NPA holographic displays, Sun *et al.* [57] propose two novel methods. The first method integrates deconvolution into each step of the iterative phase retrieval algorithm. The second method uses the proximal algorithm to find the phase-only Fourier hologram that minimizes the difference of the formed image under the thermal proximity effect and the desired 2D image through optimization. In this paper, we address the proximity effect correction on Fresnel holograms which is more practical and critical to displaying 3D scenes and objects.

3 NPA Holographic Display

This section explains the thermal phase modulation of NPAs and how the thermal proximity effect is modeled. To the best of our knowledge, the NPAs are in the design and prototyping stage. The designs of various NPAs and the differences among them are beyond the scope of this paper. We refer readers to Sun *et al.* [56] and Raval *et al.* [50] for more information.

3.1 Phase Modulation

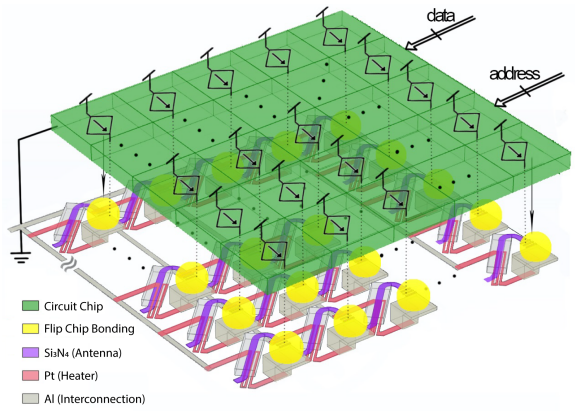

Figure 3: The NPA display with the electronic and the optical layers

The schematic of our NPA design is shown in Fig. 3. Every pixel consists of a tunable thermo-optical phase shifter and an optical

antenna. The thermal phase modulation works by adjusting the refractive index of the phase shifter with temperature. The light source is coupled into the phased array via an optic fiber and evenly distributed to the antenna of each pixel. As a result, the wavefront formed on the NPA has uniform amplitude. This means the hologram has to be phase only.

The thermal phase modulation can be expressed in the linear equation in Equation 1, where ϕ_j is the phase of pixel j and $T_j \in \mathbb{R}^+$ is its temperature above the ambient temperature.

$$\phi_j = \gamma T_j \tag{1}$$

The electric-thermal simulation on our NPA design shows that the γ values for the red (630 nm), green (530 nm), and blue (445 nm) light are $\frac{\pi}{175}$ rad °C^{-1}, $\frac{\pi}{147}$ rad °C^{-1}, and $\frac{\pi}{124}$ rad °C^{-1}, respectively.

3.2 Thermal Proximity Effect

The thermal proximity effect occurs because heating one pixel to a temperature corresponding to a certain phase value would affect the temperature of other pixels in its surroundings. Similar processes exist in other fields such as E-beam lithography and LCoS SLM holography. Similar to Peckerar *et al.* [45] and Persson *et al.* [48], we model the thermal proximity effect in NPAs as a convolution in Equation 2. T is the 2D input temperature profile of the entire NPA before considering the proximity effect. $\hat{T}$ is the 2D temperature profile of the entire NPA considering the proximity effect. K is the convolution kernel and $*$ indicates the convolution operation.

$$\hat{T} = T * K_\sigma \tag{2}$$

Specifically, the electric-thermal simulation shows that the thermal proximity effect can be modelled as a Gaussian convolution where the convolution kernel is $K = K_\sigma$ in Equation 3. $d(i,j) = \sqrt{(i-m)^2 + (j-n)^2}$ is the distance between the element at (i,j) and the center element at (m,n) measured in pixels.

$$K_\sigma(i,j) = e^{-\frac{d(i,j)^2}{\sigma^2}} \tag{3}$$

Many factors could affect the convolution, such as the pixel density and the thermal properties of the materials of the NPA. σ can be used to characterize the severity of the proximity effect. We derive $\sigma = 0.66$ px based on our simulation. We use the kernel of size 7×7. In Section 5, we show the images formed under the thermal proximity effect for varying degrees of severity.

4 Fresnel Proximity Effect Correction

Here, we present a novel proximity effect correction method for Fresnel holograms on the NPAs. We refer to this method as *Fresnel Proximity Effect Correction* (FPEC). This method uses the proximal algorithm to compute the phase of a phase-only hologram that minimizes the difference between the desired image and the image formed at a specific distance under the proximity effect. Since the mapping between the temperature and phase is linear, we directly consider the proximity effect and the correction for the phase instead of the temperature for simplicity.

Since our method focuses on Fresnel holograms and reconstructing 2D images or 3D scenes, we consider the case of Fresnel diffraction approximation. Assuming a wavefront E_1 is on the NPA, the wavefront E_2 formed by propagating E_1 by a distance z can be calculated as in Equation 4. The two wavefronts E_1 and E_2 are parallel to each other. $\mathcal{F}$ and $\mathcal{F}^{-1}$ are the Fourier transform and its inverse. $H_{z\lambda}(f_X, f_Y) = e^{ikz} \cdot e^{-i\pi\lambda z(f_X^2 + f_Y^2)}$ is the transfer function in the frequency domain where $k = \frac{2\pi}{\lambda}$ is the wave number for wavelength λ. We refer interested readers to Goodman [14] or Voelz [58] for a detailed derivation of the Fresnel diffraction.

$$E_2(x,y) = \mathcal{F}^{-1}\{\mathcal{F}[E_1(x,y)]H_{z\lambda}(f_X, f_Y)\} \tag{4}$$

Given the desired image $I \in \mathbb{R}^{+M\times N}$, we wish to find the non-negative phase $X \in \mathbb{R}^{+M\times N}$ that minimizes the difference between the desired image I and the formed image under the proximity effect, expressed as $g(X)$ in Equation 5. Let $P(X)$ be the function that applies the proximity effect to the phase pattern, i.e. $E_1 = e^{iP(X)}$ and $P(X) = X * K$ where K is the convolution kernel in Equation 2. Let $U(X)$ be the intensity of the wavefront which the NPA with input phase X forms at a specific distance z from the NPA, $U(X) = |E_2|^2$.

$$g(X) = \|U(X) - I\|_{\mathrm{F}}^2 \tag{5}$$

$$U(X) = |\mathcal{F}^{-1}[\mathcal{F}(e^{iP(X)})H_{z\lambda}]|^2 \tag{6}$$

We use an indicator function $c(X)$ that penalizes negative entries to ensure a non-negative solution. The cost function $f(X)$ is defined as follows:

$$f(X) = g(X) + c(X) \tag{7}$$

$$c(X) = \mathcal{I}_{[0,+\inf)}(X) \tag{8}$$

The FPEC method minimizes the function $f(X)$ in Equation 7 using the accelerated proximal algorithm.

The pseudocode of the FPEC method is shown in Algorithm 1. ω is an extrapolation coefficient which is used to make the algorithm converge faster. We use the simple choice of $\omega = \frac{k}{k+3}$ suggested in Parikh and Boyd [44] where k is the iteration number. $\tau \in \mathbb{R}^+$ is the step size of the proximal operator $\mathrm{prox}_{\tau c}(Y - \tau\nabla g(Y))$ defined in Equation 9.

$$\mathrm{prox}_{\tau c}(Y - \tau\nabla g(Y)) = \underset{X}{\mathrm{argmin}}\{c(X) + \frac{1}{2\tau}\|X - (Y - \tau\nabla g(Y))\|_2^2\} \tag{9}$$

$g'_\tau(Z,Y) = g(Y) + \mathrm{tr}(\nabla g(Y)(Z-Y))^T + \frac{1}{2\tau}\|Z-Y\|_{\mathrm{F}}^2$ and $\beta \in (0,1)$ are used in the line search method (Beck and Teboulle [2]) to adjust the step size τ.

The termination condition is met when the $g(X)$ difference between iterations becomes small. Specifically, we terminate the iterations when the residual change r^k defined in Equation 10 is smaller than a predefined threshold. X^k is the solution in iteration k.

$$r_k = \frac{\mathrm{abs}(g(X^k) - g(X^{k-1}))}{g(X^{k-1})} \tag{10}$$

The derivative ∇g of the function $g(X)$ can be computed as in Equation 11. The technical derivation is provided in the supplemental material.

$$\nabla g = 4\mathrm{Re}(S) \tag{11}$$

$$S = P(ie^{iP} \cdot \mathcal{F}\{H \cdot [\mathcal{F}^{-1}(Q \cdot F)]\}) \tag{12}$$

$$Q = U - I \tag{13}$$

$$F = \mathcal{F}^{-1}[\mathcal{F}(e^{iP(X)})H] \tag{14}$$

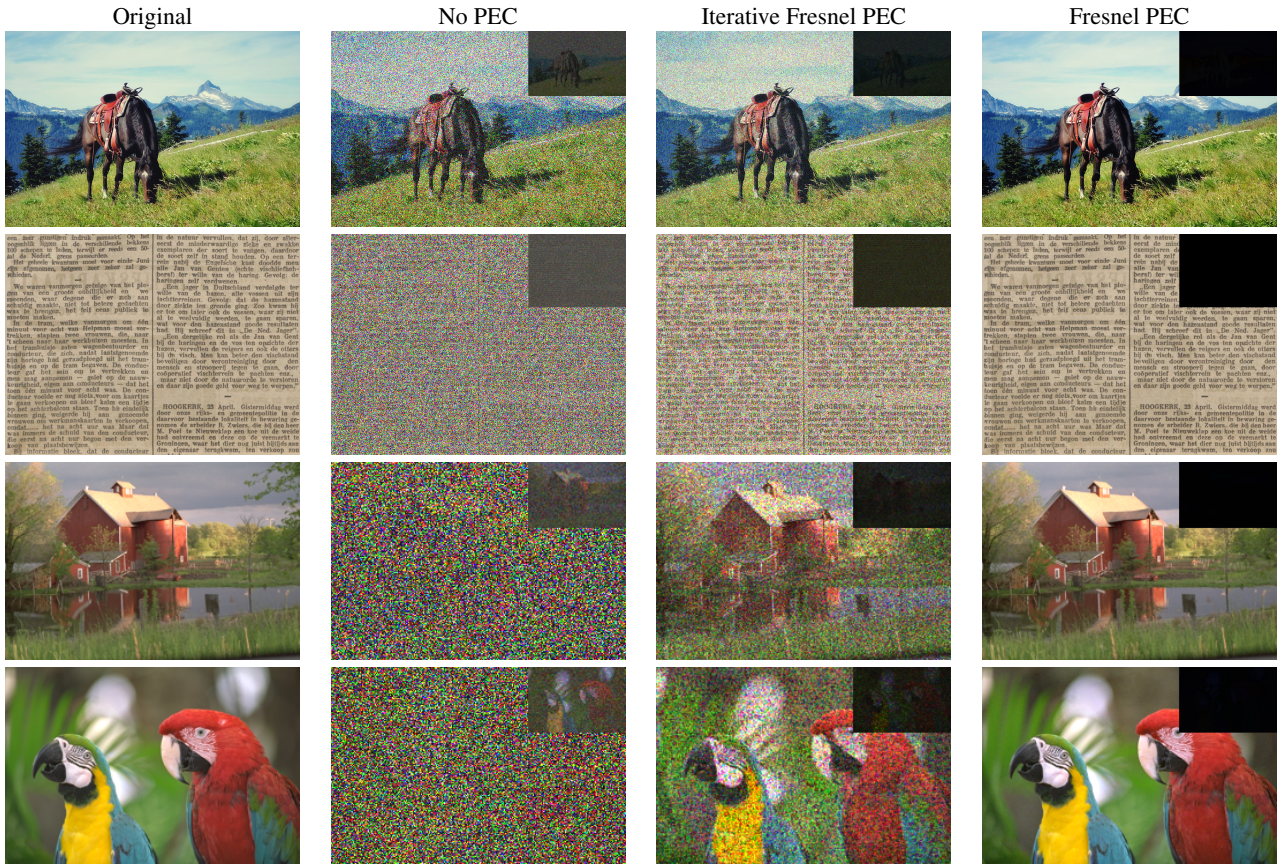

Figure 4: Qualitative comparison of the Fresnel PEC method with the case without proximity effect correction and the iterative Fresnel PEC method. The original image is presented in the left column for reference. The absolute difference between the reconstructed image and the original is shown in each image. The thermal proximity effect levels for the images from top to bottom are $\sigma = 0.70$ px, 0.80 px, 0.90 px and 1.00 px, respectively. At $\sigma = 0.70$ px, the proximity effect causes noise but the images are still recognizable. However, for more severe proximity effect, the noise overwhelms the images. Our Fresnel PEC method is able to correct the proximity effect and restore the images close to the original even at such high proximity effect levels. The images in the first and second rows are from the Common Objects in Context dataset [29] and the CHRONIC dataset (Smits and Faber [54]), respectively. The remaining images are from the LIVE dataset (Sheikh *et al.* [51, 52]).

5 Simulations

We present computational simulations of our novel Fresnel PEC method. We conduct the simulations on Matlab on a PC with an Intel 9900K CPU. We use wavelengths $630\,\mathrm{nm}$, $530\,\mathrm{nm}$, and $445\,\mathrm{nm}$ for the red, green, and blue channels. We use color images as the proposed Fresnel PEC method is applicable to all wavelengths and color switching can be easily realized by coupling multiple light sources into the NPA. The NPA is assumed to have the pixel pitch of $0.01\,\mathrm{mm}$ and the same resolution as the image. The images are placed $100\,\mathrm{mm}$ away from NPA. We terminate the iterations when r_k in Equation 10 remains below 0.001 for 10 iterations.

We compare the proposed Fresnel PEC method with two baselines. The first is the case without proximity effect correction where the proximity effect is applied to the phase of the phase-only hologram. The second is based on the Iterative Proximity Effect Correction (IPEC) method in Sun *et al.* [57] which improves upon the iterative method from Persson *et al.* [48] and Gemayel *et al.* [12]. In this method, we replace the wavefront propagation with the Fresnel propagation approximation to make it compatible with the Fresnel holograms. We refer to this method as the *Iterative Fresnel Proximity Effect Correction* (IFPEC) method.

5.1 2D Fresnel Holograms

The qualitative results of the FPEC on 2D images are shown in Fig. 4. As can be seen, the proximity effect results in appreciable noise in the simulated images. The proximity effect levels in Fig. 4 are $\sigma = 0.70$ px, 0.80 px, 0.90 px, and 1.00 px in the four rows from top to bottom, respectively. For the two baseline methods, the higher the proximity effect, the noisier the images become. We also show the noise mask as the absolute difference between the reconstructed image and the original image as the insets. As can be seen, the noise due to the proximity effect depends on the original image and is becomes more prominent with higher proximity effect levels. Our proposed FPEC method is able to effectively reduce the noise caused by the proximity effect even at very high proximity effect levels. Compared with the IFPEC method, our method is able to better correct the proximity effect and restore the images.

In addition to qualitative reconstructions of the images, we also quantify our results with the *structural similarity index* (SSIM) from Wang *et al.* [67] and the *perceptual similarity* from Zhang *et al.* [65]. SSIM is a well-known image quality metric. The power of the luminance, contrast, and structure terms we use are all 1. When the image in question is identical to the reference image, SSIM $= 1$. As the image quality decreases, so does SSIM. Zhang *et al.* [65] find that some of the loss functions based on the deep features of image synthesis applications are uniquely suited for expressing the image

Algorithm 1: Fresnel Proximity Effect Correction

input : X_0, I, ω, τ, β
output : X
$X = X_0$;
$X_{\text{prev}} = X$;
while *Within maximum iteration* **do**
  $Y = X + \omega(X - X_{\text{prev}})$;
  while *true* **do**
    $Z = \text{prox}_{\tau c}(Y - \tau \nabla g(Y))$;
    if $g(Z) < g'_{\tau}(Z, Y)$ **then**
      break;
    else
      $\tau = \beta\tau$;
    end
  end
  $X_{\text{prev}} = X$;
  $X = Z$;
  if *Termination condition met* **then**
    break;
  end
end

quality. The metric d produced by their network[2] represents the *perceptual difference*. To stay consistent with the SSIM scale, where larger metric value means better image quality, we use $s = e^{-d}$ to express the *perceptual similarity*.

We present the average image metrics of the images from the LIVE dataset from Sheikh *et al.* [51,52] at proximity effect levels from $\sigma = 0.10$ px to 1.00 px. As can be seen, the proposed FPEC method can effectively correct the proximity effect from $\sigma = 0.10$ px to 0.90 px, with only a slight dip in the image quality at $\sigma = 1.00$ px. As a comparison, the case without PEC starts to see rapid image quality degradation starting from $\sigma = 0.30$ px, and the iterative Fresnel PEC method suffers from noise starting from $\sigma = 0.40$ px. The two image metrics are largely consistent with each other with the exception of the iterative Fresnel PEC method at proximity effect levels at $\sigma = 0.90$ px and 1.00 px. In this case, we think that the perceptual similarity represents the image quality better. Some examples of such mismatch between the two image metrics can be seen in the supplemental material.

5.2 3D Scenes using Time-Division Multiplexing

The Fresnel PEC method can effectively correct 2D Fresnel holograms formed at desired depths. This can be used in combination with the fast refresh rate of the NPA to display 3D scenes. A 3D scene can be divided into a stack of 2D images at different depths. The 2D Fresnel hologram of each image can be calculated and the proximity effect corrected with the Fresnel PEC method at the desired depth. The stack of holograms can be displayed on the NPA in consecutive frames using time-division multiplexing so that the 3D scene can be observed.

We present the simulations of such 3D holograms[3] in Fig. 6. A 3D volume is divided into a stack of images whose 2D Fresnel holograms are calculated at their respective depths with the Fresnel PEC method. Those holograms are reconstructed by propagating the wavefronts formed at the holograms to a certain distance from the NPA that corresponds to the user's focal plane. The average of those reconstructions is taken as the observation. Holograms of 3D meshes and point clouds can be computed and displayed in a similar

[2] https://github.com/richzhang/PerceptualSimilarity

[3] Volumes are from https://klacansky.com/open-scivis-datasets and http://www.sci.utah.edu/download/IV3DData.html

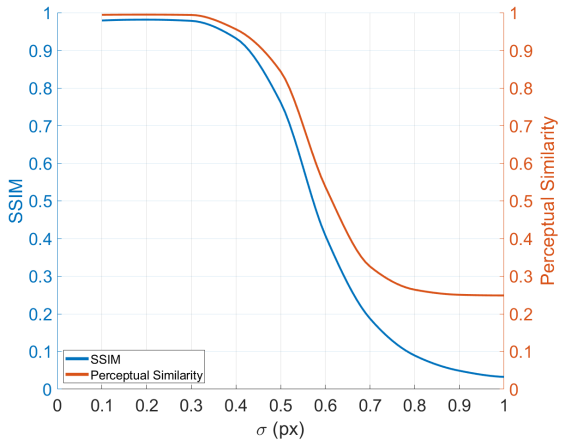

No PEC

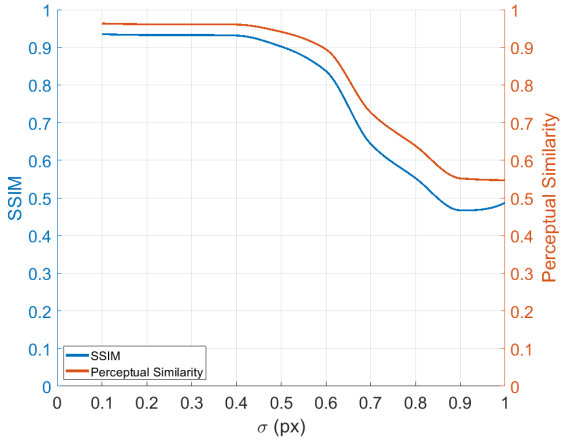

Iterative Fresnel PEC

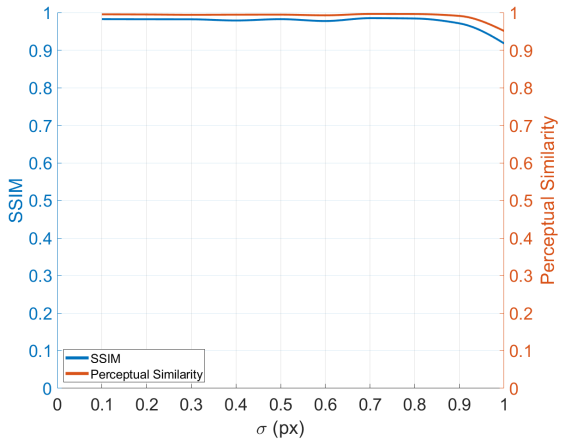

Fresnel PEC

Figure 5: The SSIM and perceptual similarity of the Fresnel PEC results compared to the case without proximity effect correction and the iterative Fresnel PEC (IFPEC) method. When there is no PEC, the image quality degrades quickly with the proximity effect level beyond $\sigma = 0.30$ px. The image quality of the IFPEC method starts to degrade starting from $\sigma = 0.40$ px. The Fresnel PEC method can effectively correct the proximity effect at almost all proximity effect levels tested, only to see image quality degrade slightly at extreme proximity effect level $\sigma = 1.00$ px.

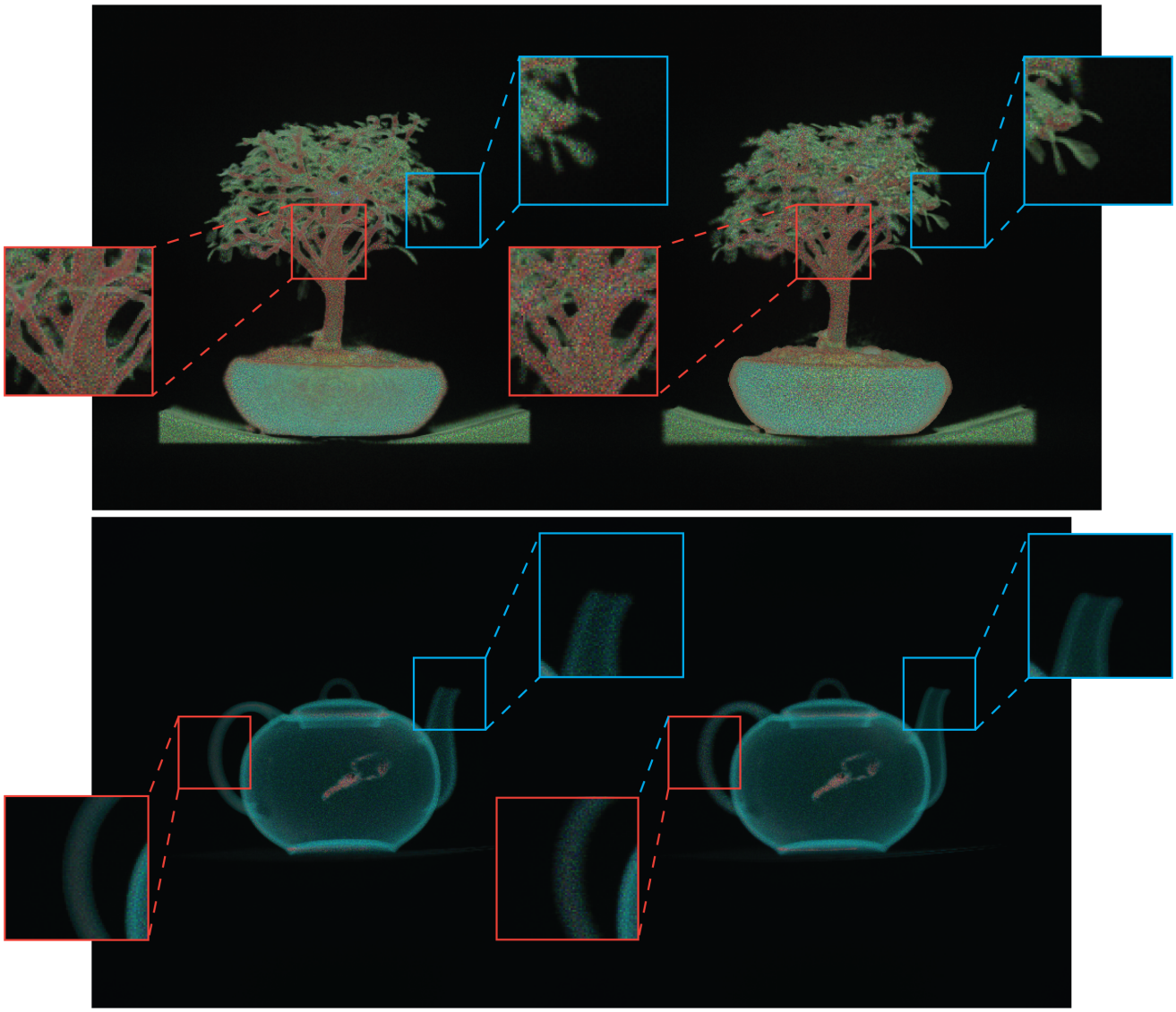

Figure 6: The 3D volume is divided into a stack of images at different depths. The Fresnel holograms of all the images are calculated with the Fresnel PEC method at their respective depths and displayed on the NPA in consecutive frames so the 3D scene can be observed. We simulate the observation by reconstructing the holograms at a certain distance that corresponds to the user's focal plane. By adjusting the focal plane (for example, the focal plane used in the left image is on the front part of the object while the focal plane used in the right image is on the back part of the object), different parts of the scene (red or blue inset) are in focus. The top and bottom volumes are divided into 232 and 253 equidistant slices, respectively. The proximity effect level used is $\sigma = 0.66$ px.

$\sigma = 1.50$ px $\sigma = 2.00$ px

Figure 7: The FPEC method at higher proximity effect levels where much noise is observed.

way. The user can focus on different parts of the 3D scene. We simulate this by adjusting the focal plane accordingly.

6 Discussions and Future Work

Here we discuss some limitations of our proposed Fresnel PEC method and propose several directions for future research.

6.1 Larger Proximity Effect

We have shown in our simulations that the proposed Fresnel PEC method is effective within the tested proximity effect level range ($\sigma = 0.10$ px to 1.00 px). While this is a large and realistic range where most NPAs including our design fall, it is not difficult to imagine cases where a more severe proximity effect may arise. For example, as the pixels on the NPA are more densely packed, it can be expected that each pixel is affected more by nearby pixels. In Fig. 5, we see that the image quality of the Fresnel PEC results starts to decrease at $\sigma = 1.00$ px. At higher proximity effect levels, the image quality would drop more. At proximity effect levels $\sigma = 1.50$ px and 2.00 px, the average SSIMs of the results of FPEC are 0.57 and 0.34 while the average perceptual similarities are 0.69 and 0.48. Examples of the FPEC method at higher proximity effect levels can be seen in Fig. 7.

6.2 Processing Time

The Fresnel PEC method is an iterative algorithm. Currently, it takes our implementation 4.28 s to process a 256×256 image at proximity effect level $\sigma = 0.66$ px. However, the Fresnel PEC method is on average 36.18 times faster than the Iterative Fresnel PEC method while also offering a superior correction effectiveness. Since the Fresnel PEC method heavily uses the Fourier transform, we believe that hardware implementation and massive parallelization can significantly accelerate it. A naive translation to CUDA has yielded a $15\times$ speedup on an Nvidia RTX 2080Ti GPU. Special hardware for the Fourier transform such as the on-chip integrated all-optical FFT with a 26 Tbps data throughput by Nejadriahi and Sorger [40] may also significantly increase the speed of this method. Alternatively, it is desirable to investigate how to properly adjust the convergence condition and the step size for maximum efficiency.

Deep neural networks may also be uniquely suitable for accelerating the proximity effect correction. Deep neural networks not only have a fixed complexity compared to the iterative proximal algorithms, but they can also encode the proximity effect as part of the light transportation model such as shown in Peng *et al.* [47].

6.3 3D Fresnel Holograms

In this work, we demonstrated displaying 3D holograms by using time-division multiplexing to display multiple 2D Fresnel holograms processed with the Fresnel PEC method at different depths in consecutive frames. Proximity effect correction on 3D Fresnel holograms where one hologram encodes the entire 3D scene will be an interesting direction for future work. A naive solution would be to calculate the fully complex or phase-only 3D Fresnel hologram similar to Shi *et al.* [53] and Maimone *et al.* [34] and perform deconvolution on the phase signal. The non-negative constraint needs to be enforced in the deconvolution. An alternative is to optimize the observed 3D scene similar to the proposed Fresnel PEC method. It remains to be seen how to define the cost function similar to Equation 5 for a 3D scene.

7 Conclusion

The NPAs as holographic displays have the advantages of a small form factor due to integrated light source and a high refresh rate. One challenge facing the NPA is the thermal proximity effect present in all thermally-modulated NPAs. In this work, we present the Fresnel proximity effect correction method that can correct the thermal proximity effect for Fresnel holograms on the NPAs. Compared to the previous PEC methods for Fourier holograms, this method can specify where the observed image forms. By adjusting where the Fresnel holograms forms the observed images and making use of the fast refresh rate of the NPAs, we can use the time-division multiplexing techniques to display 3D scenes on the NPA. We believe that our approach is the first that addresses the proximity effect correction for Fresnel holograms and makes a meaningful contribution to the emerging field of NPAs. We hope that it brings this highly interesting technology for holographic displays closer to practical use.

Acknowledgement

We would like to thank the anonymous reviewers for the helpful comments. We also greatly appreciate the insightful suggestions by Ward Lopes and David Luebke from NVIDIA. This work has been supported in part by the NSF Grants 15-64212, 18-23321, and the State of Maryland's MPower initiative. Any opinions, findings, conclusions, or recommendations expressed in this article are those of the authors and do not necessarily reflect the views of the research sponsors.

References

[1] K. Akşit, W. Lopes, J. Kim, P. Shirley, and D. Luebke. Near-eye varifocal augmented reality display using see-through screens. *ACM Transactions on Graphics (TOG)*, 36(6):189, 2017.

[2] A. Beck and M. Teboulle. Gradient-based algorithms with applications to signal recovery. *Convex optimization in signal processing and communications*, pp. 42–88, 2009.

[3] P. Chakravarthula, D. Dunn, K. Akşit, and H. Fuchs. FocusAR: Auto-focus augmented reality eyeglasses for both real world and virtual imagery. *IEEE Transactions on Visualization and Computer Graphics*, 24(11):2906–2916, 2018.

[4] P. Chakravarthula, Y. Peng, J. Kollin, H. Fuchs, and F. Heide. Wirtinger holography for near-eye displays. *ACM Trans. Graph.*, 38(6), Nov. 2019. doi: 10.1145/3355089.3356539

[5] P. Chakravarthula, Y. Peng, J. Kollin, F. Heide, and H. Fuchs. Computing high quality phase-only holograms for holographic displays. In B. C. Kress and C. Peroz, eds., *Optical Architectures for Displays and Sensing in Augmented, Virtual, and Mixed Reality (AR, VR, MR)*, vol. 11310, pp. 47 – 62. International Society for Optics and Photonics, SPIE, 2020. doi: 10.1117/12.2547647

[6] J. Chen, L. Mi, C. P. Chen, H. Liu, J. Jiang, and W. Zhang. Design of foveated contact lens display for augmented reality. *Opt. Express*, 27(26):38204–38219, Dec 2019. doi: 10.1364/OE.381200

[7] J. K. Doylend, M. J. R. Heck, J. T. Bovington, J. D. Peters, L. A. Coldren, and J. E. Bowers. Two-dimensional free-space beam steering with an optical phased array on silicon-on-insulator. *Opt. Express*, 19(22):21595–21604, Oct 2011. doi: 10.1364/OE.19.021595

[8] D. Dunn, C. Tippets, K. Torell, P. Kellnhofer, K. Akşit, P. Didyk, K. Myszkowski, D. Luebke, and H. Fuchs. Wide field of view varifocal near-eye display using see-through deformable membrane mirrors. *IEEE Transactions on Visualization and Computer Graphics*, 23(4):1322–1331, 2017.

[9] M. H. Eybposh, N. W. Caira, M. Atisa, P. Chakravarthula, and N. C. Pégard. DeepCGH: 3D computer-generated holography using deep learning. *Opt. Express*, 28(18):26636–26650, Aug ts , url = http://www.opticsexpress.org/abstract.cfm?URI=oe-28-18-26636, doi = 10.1364/OE.399624,.

[10] R. Fatemi, B. Abiri, A. Khachaturian, and A. Hajimiri. High sensitivity active flat optics optical phased array receiver with a two-dimensional aperture. *Opt. Express*, 26(23):29983–29999, Nov 2018. doi: 10.1364/OE.26.029983

[11] A. J. Fenn, D. H. Temme, W. P. Delaney, and W. E. Courtney. The development of phased-array radar technology. *Lincoln Laboratory Journal*, 12(2):321–340, 2000.

[12] P. Gemayel, B. Colicchio, A. Dieterlen, and P. Ambs. Cross-talk compensation of a spatial light modulator for iterative phase retrieval applications. *Applied optics*, 55(4):802–810, 2016.

[13] R. W. Gerchberg and W. O. Saxton. A practical algorithm for the determination of phase from image and diffraction plane pictures. *Optik*, 35:237–246, 1972.

[14] J. W. Goodman. *Introduction to Fourier optics*. Roberts and Company Publishers, 2005.

[15] D. M. Hoffman, A. R. Girshick, K. Akeley, and M. S. Banks. Vergence–accommodation conflicts hinder visual performance and cause visual fatigue. *Journal of Vision*, 8(3):33–33, 03 2008. doi: 10.1167/8.3.33

[16] H. Ikeda, T. Hayakawa, and M. Ishikawa. Bilateral motion display: Strategy to provide multiple visual perception using afterimage effects for specific motion. In *25th ACM Symposium on Virtual Reality Software and Technology*, VRST '19. Association for Computing Machinery, New York, NY, USA, 2019. doi: 10.1145/3359996.3364241

[17] C. Jang, K. Bang, G. Li, and B. Lee. Holographic near-eye display with expanded eye-box. *ACM Trans. Graph.*, 37(6), Dec. 2018. doi: 10.1145/3272127.3275069

[18] M. A. Khalighi and M. Uysal. Survey on free space optical communication: A communication theory perspective. *IEEE Communications Surveys Tutorials*, 16(4):2231–2258, 2014.

[19] J. Kim, Y. Jeong, M. Stengel, K. Akşit, R. Albert, B. Boudaoud, T. Greer, J. Kim, W. Lopes, Z. Majercik, P. Shirley, J. Spjut, M. McGuire, and D. Luebke. Foveated AR: Dynamically-foveated augmented reality display. *ACM Trans. Graph.*, 38(4):99:1–99:15, July 2019. doi: 10.1145/3306346.3322987

[20] K. Kiyokawa. A wide field-of-view head mounted projective display using hyperbolic half-silvered mirrors. In *Proceedings of the 2007 6th IEEE and ACM International Symposium on Mixed and Augmented Reality*, ISMAR '07, pp. 1–4. IEEE Computer Society, Washington, DC, USA, 2007. doi: 10.1109/ISMAR.2007.4538848

[21] G. A. Koulieris, K. Akşit, M. Stengel, R. K. Mantiuk, K. Mania, and C. Richardt. Near-eye display and tracking technologies for virtual and augmented reality. *Computer Graphics Forum*, 38(2):493–519, 2019. doi: 10.1111/cgf.13654

[22] G. Kramida. Resolving the vergence-accommodation conflict in head-mounted displays. *IEEE Transactions on Visualization and Computer Graphics*, 22(7):1912–1931, 2016.

[23] G. Kuo, L. Waller, R. Ng, and A. Maimone. High resolution étendue expansion for holographic displays. *ACM Trans. Graph.*, 39(4), July 2020. doi: 10.1145/3386569.3392414

[24] D. Lanman and D. Luebke. Near-eye light field displays. *ACM Transactions on Graphics (TOG)*, 32(6):220, 2013.

[25] D. Lee and H. S. Seung. Algorithms for non-negative matrix factorization. In T. Leen, T. Dietterich, and V. Tresp, eds., *Advances in Neural Information Processing Systems*, vol. 13, pp. 556–562. MIT Press, 2001.

[26] S. Lee, C. Jang, S. Moon, J. Cho, and B. Lee. Additive light field displays: Realization of augmented reality with holographic optical elements. *ACM Trans. Graph.*, 35(4):60:1–60:13, July 2016. doi: 10.1145/2897824.2925971

[27] S. Lee, C. Jang, S. Moon, B. Lee, J. Cho, and B. Lee. See-through light field displays for augmented reality. In *SIGGRAPH ASIA 2016 Virtual Reality Meets Physical Reality: Modelling and Simulating Virtual Humans and Environments*, SA '16, pp. 3:1–3:2. ACM, New York, NY, USA, 2016. doi: 10.1145/2992138.2992142

[28] P. Li. A review of proximity effect correction in electron-beam lithography. *arXiv preprint arXiv:1509.05169*, 2015.

[29] T.-Y. Lin, M. Maire, S. Belongie, J. Hays, P. Perona, D. Ramanan, P. Dollár, and C. L. Zitnick. Microsoft coco: Common objects in context. In D. Fleet, T. Pajdla, B. Schiele, and T. Tuytelaars, eds., *Computer Vision – ECCV 2014*, pp. 740–755. Springer International Publishing, Cham, 2014.

[30] A. Lohmann and D. Paris. Synthesis of binary holograms. *IEEE Journal of Quantum Electronics*, 2(4):153–153, 1966.

[31] M. E. Lucente. Interactive computation of holograms using a look-up table. *Journal of Electronic Imaging*, 2(1):28–35, 1993.

[32] M. E. Lucente and T. A. Galyean. Rendering interactive holographic images. In *Proceedings of the 22nd annual conference on Computer graphics and interactive techniques*, pp. 387–394. ACM, 1995.

[33] A. Maimone and H. Fuchs. Computational augmented reality eyeglasses. In *2013 IEEE International Symposium on Mixed and Augmented Reality (ISMAR)*, pp. 29–38. IEEE, 2013.

[34] A. Maimone, A. Georgiou, and J. S. Kollin. Holographic near-eye displays for virtual and augmented reality. *ACM Transactions on Graphics (TOG)*, 36(4):85, 2017.

[35] A. Maimone, D. Lanman, K. Rathinavel, K. Keller, D. Luebke, and H. Fuchs. Pinlight displays: wide field of view augmented reality eyeglasses using defocused point light sources. In *ACM SIGGRAPH 2014 Emerging Technologies*, p. 20. ACM, 2014.

[36] C. R. Marrian, S. Chang, and M. C. Peckerar. Proximity correction for electron beam lithography. *Optical Engineering*, 35(9):2685–2693, 1996.

[37] L. Mi, C. P. Chen, Y. Lu, W. Zhang, J. Chen, and N. Maitlo. Design of lensless retinal scanning display with diffractive optical element. *Opt. Express*, 27(15):20493–20507, Jul 2019. doi: 10.1364/OE.27.020493

[38] S. A. Miller, C. T. Phare, Y.-C. Chang, X. Ji, O. A. J. Gordillo, A. Mohanty, S. P. Roberts, M. C. Shin, B. Stern, M. Zadka, and M. Lipson. 512-element actively steered silicon phased array for low-power lidar. In *Conference on Lasers and Electro-Optics*, p. JTh5C.2. Optical Society of America, 2018.

[39] H. Nagahara, Y. Yagi, and M. Yachida. Super wide viewer using catadioptrical optics. In *Proceedings of the ACM Symposium on Virtual Reality Software and Technology*, VRST '03, pp. 169–175. ACM, New York, NY, USA, 2003. doi: 10.1145/1008653.1008683

[40] H. Nejadriahi and V. J. Sorger. On-chip integrated all-optical fast fourier transform: Design and analysis. In *Frontiers in Optics 2017*, p. JW4A.46. Optical Society of America, 2017. doi: 10.1364/FIO.2017.JW4A.46

[41] J. Notaros, M. Raval, M. Notaros, and M. R. Watts. Integrated-phased-array-based visible-light near-eye holographic projector. p. STu3O.4. Optical Society of America, 2019.

[42] N. Padmanaban, Y. Peng, and G. Wetzstein. Holographic near-eye displays based on overlap-add stereograms. *ACM Trans. Graph.*, 38(6), Nov. 2019. doi: 10.1145/3355089.3356517

[43] M. Parikh. Corrections to proximity effects in electron beam lithography. i. theory. *Journal of Applied Physics*, 50(6):4371–4377, 1979.

[44] N. Parikh and S. Boyd. Proximal algorithms. *Foundations and Trends® in Optimization*, 1(3):127–239, 2014. doi: 10.1561/2400000003

[45] M. Peckerar, R. Bass, and K. W. Rhee. Sub-0.1 μ electron-beam lithography for nanostructure development. *Journal of Vacuum Science & Technology B: Microelectronics and Nanometer Structures Processing, Measurement, and Phenomena*, 18(6):3143–3149, 2000.

[46] M. C. Peckerar, S. Chang, and C. R. K. Marrian. Proximity correction algorithms and a co-processor based on regularized optimization. i. description of the algorithm. *Journal of Vacuum Science & Technology B: Microelectronics and Nanometer Structures Processing, Measurement, and Phenomena*, 13(6):2518–2525, 1995. doi: 10.1116/1.588385

[47] Y. Peng, S. Choi, N. Padmanaban, J. Kim, and G. Wetzstein. Neural holography with camera-in-the-loop training. *ACM Transactions on Graphics (TOG)*, 39(6), 2020.

[48] M. Persson, D. Engström, and M. Goksör. Reducing the effect of pixel crosstalk in phase only spatial light modulators. *Optics express*, 20(20):22334–22343, 2012.

[49] C. V. Poulton, A. Yaacobi, D. B. Cole, M. J. Byrd, M. Raval, D. Vermeulen, and M. R. Watts. Coherent solid-state lidar with silicon pho-

tonic optical phased arrays. *Opt. Lett.*, 42(20):4091–4094, Oct 2017. doi: 10.1364/OL.42.004091

[50] M. Raval, A. Yaacobi, and M. R. Watts. Integrated visible light phased array system for autostereoscopic image projection. *Opt. Lett.*, 43(15):3678–3681, Aug 2018. doi: 10.1364/OL.43.003678

[51] H. R. Sheikh, M. F. Sabir, and A. C. Bovik. A statistical evaluation of recent full reference image quality assessment algorithms. *IEEE Transactions on Image Processing*, 15(11):3440–3451, Nov 2006. doi: 10.1109/TIP.2006.881959

[52] H. R. Sheikh, Z. Wang, L. Cormack, and A. C. Bovik. Live image quality assessment database release 2. `http://live.ece.utexas.edu/research/quality`, 2004. Accessed: 2019-04-03.

[53] L. Shi, F.-C. Huang, W. Lopes, W. Matusik, and D. Luebke. Near-eye light field holographic rendering with spherical waves for wide field of view interactive 3D computer graphics. *ACM Transactions on Graphics (TOG)*, 36(6):236, 2017.

[54] T. Smits and W. Faber. Chronic (classified historical newspaper images). KB Lab: The Hague. `http://lab.kb.nl/dataset/chronic-classified-historical-newspaper-images`, 2018.

[55] S. J. Spector, B. F. Lane, M. R. Watts, L. D. Benney, J. G. Delva, A. E. Hare, A. F. Kelsey, J. M. Mlynarczyk, E. S. Hosseini, C. V. Poulton, and J. P. Laine. Broadband imaging and wireless communication with an optical phased array. In *Conference on Lasers and Electro-Optics*, p. SM3I.7. Optical Society of America, 2018. doi: 10.1364/CLEO_SI.2018.SM3I.7

[56] J. Sun, E. Timurdogan, A. Yaacobi, E. S. Hosseini, and M. R. Watts. Large-scale nanophotonic phased array. *Nature*, 493(7431):195, 2013.

[57] X. Sun, Y. Zhang, P. C. Huang, N. Acharjee, M. Dagenais, M. Peckerar, and A. Varshney. Correcting the proximity effect in nanophotonic phased arrays. *IEEE Transactions on Visualization and Computer Graphics*, 26(12):3503–3513, 2020. doi: 10.1109/TVCG.2020.3023601

[58] D. Voelz. Computational fourier optics: a matlab tutorial. Society of Photo-Optical Instrumentation Engineers, 2011.

[59] Z. Wang, X. Jin, F. Xue, R. Li, H. Zha, and K. Ikeuchi. Perceptual enhancement for stereoscopic videos based on horopter consistency. In *Proceedings of the 22nd ACM Conference on Virtual Reality Software and Technology*, VRST '16, p. 15–18. Association for Computing Machinery, New York, NY, USA, 2016. doi: 10.1145/2993369.2993393

[60] G. Wetzstein, D. Lanman, M. Hirsch, and R. Raskar. Tensor displays: Compressive light field synthesis using multilayer displays with directional backlighting. *ACM Trans. Graph.*, 31(4), July 2012. doi: 10.1145/2185520.2185576

[61] X. Xia, Y. Guan, A. State, P. Chakravarthula, K. Rathinavel, T. Cham, and H. Fuchs. Towards a switchable AR/VR near-eye display with accommodation-vergence and eyeglass prescription support. *IEEE Transactions on Visualization and Computer Graphics*, 25(11):3114–3124, 2019.

[62] S. Xu, F. Farbiz, S. Solanki, X. Liang, and X. Xu. Adaptive computation of computer-generated holograms. In *Proceedings of The 7th ACM SIGGRAPH International Conference on Virtual-Reality Continuum and Its Applications in Industry*, VRCAI '08, pp. 35:1–35:2. ACM, New York, NY, USA, 2008. doi: 10.1145/1477862.1477908

[63] H. Yoshikawa, S. Iwase, and T. Oneda. Fast computation of fresnel holograms employing difference. In *Practical Holography XIV and Holographic Materials VI*, vol. 3956, pp. 48–56. International Society for Optics and Photonics, 2000.

[64] H. Yu, M. Bemana, M. Wernikowski, M. Chwesiuk, O. T. Tursun, G. Singh, K. Myszkowski, R. Mantiuk, H. Seidel, and P. Didyk. A perception-driven hybrid decomposition for multi-layer accommodative displays. *IEEE Transactions on Visualization and Computer Graphics*, 25(5):1940–1950, 2019.

[65] R. Zhang, P. Isola, A. A. Efros, E. Shechtman, and O. Wang. The unreasonable effectiveness of deep features as a perceptual metric. In *2018 IEEE/CVF Conference on Computer Vision and Pattern Recognition*, pp. 586–595, 2018.

[66] J. Zhou, J. Sun, A. Yaacobi, C. V. Poulton, and M. R. Watts. Design of 3D hologram emitting optical phased arrays. p. IT4A.7. Optical Society of America, 2015.

[67] Zhou Wang, A. C. Bovik, H. R. Sheikh, and E. P. Simoncelli. Image quality assessment: from error visibility to structural similarity. *IEEE Transactions on Image Processing*, 13(4):600–612, April 2004. doi: 10.1109/TIP.2003.819861